Changes to Middle East and Southwest Asia Compound Drought and Heat since 1999

ANDREW HOELL,[a] RACHEL ROBINSON,[a,b] LAURIE AGEL,[c] MATHEW BARLOW,[c] MELISSA BREEDEN,[b] JON EISCHEID,[b] AMY MCNALLY,[d] KIMBERLY SLINSKI,[d,e] AND XIAO-WEI QUAN[a,b]

[a] *NOAA Physical Sciences Laboratory, Boulder, Colorado*
[b] *Cooperative Institute for Research in Environmental Sciences, University of Colorado Boulder, Boulder, Colorado*
[c] *Department of Environmental, Earth and Atmospheric Sciences, University of Massachusetts Lowell, Lowell, Massachusetts*
[d] *NASA Goddard Space Flight Center, Greenbelt, Maryland*
[e] *Earth System Science Interdisciplinary Center, University of Maryland, College Park, College Park, Maryland*

(Manuscript received 31 March 2023, in final form 1 October 2023, accepted 5 October 2023)

ABSTRACT: We diagnose physical factors related to frequent compound drought and heat extremes over a Middle East and Southwest Asia (MESA; 30°–40°N, 35°–65°E) region in a recent (1999–2022) compared to a prior (1951–98) period. The recent compound extremes were related to conflict, disease transmission, and water shortages in this already semiarid region. Observed estimates and four transient climate model ensembles are used to identify the effect of El Niño–Southern Oscillation (ENSO) and atmospheric forcing by greenhouse gases and aerosols on these compound extremes in autumn (September–November), winter (December–February), spring (March–May), and summer (June–August) that may lead to practical forecast skill for future compound events. Observations and climate models indicate that MESA compound drought and heat in the autumn, winter, and spring wet seasons for the recent period were related to the La Niña phase of ENSO and an attendant northward shift of the storm track that hinders precipitation-bearing storms from moving through MESA. A comparison of different conditions in the model simulations is used to isolate the effects of La Niña and the atmospheric forcing by greenhouse gases and aerosols on compound MESA drought and heat. A comparison of recent and prior periods in the climate models, which isolates the effects of the atmospheric forcing, indicates that greenhouse gases and aerosols are related to the increases in MESA heat frequency in all seasons. A comparison of La Niña to ENSO neutral and El Niño in the recent period of the climate models indicates that La Niña is related to increases in MESA drought frequency in the wet seasons.

SIGNIFICANCE STATEMENT: Compound drought and heat pose serious threats to the Middle East and Southwest Asia (MESA) where political and socioeconomic challenges leave its people vulnerable to climate extremes. In this region, frequent seasonal compound drought and heat in a recent (1999–2022) compared to a prior (1951–98) period were related to conflict and water shortages. Physical factors related to these compound extremes in the recent period over MESA were identified, potentially rendering future occurrences predictable. La Niña and atmospheric forcing by greenhouse gases and aerosols contributed to the compound extremes, with the former related to anomalously low precipitation in the September–November, December–February, and March–May wet seasons and the latter related to anomalous high temperatures in all seasons, including June–August.

KEYWORDS: Drought; Heat wave; Precipitation; Climate change; La Nina; Temperature

1. Introduction

Arid and semiarid climates (Beck et al. 2018), combined with widespread political and socioeconomic challenges, leave western Asia and its people especially vulnerable to climate extremes (Agrawala et al. 2001; Kaniewski et al. 2012; Selby and Hoffmann 2012). In a recent (1999–2022) compared to a prior (1951–98) period, a Middle East and Southwest Asia (MESA) region, here defined as the area bounded by 30°–40°N and 35°–65°E, endured compound drought and heat (Fig. 1) that were associated with many negative impacts, including conflict, migration, disease transmission, water shortages, crop failures, and livestock losses (Lautze et al. 2002; Gleick 2014; Kelley et al. 2015; Barlow et al. 2016). Within this MESA region, annual precipitation decreased by 9% in the recent compared to the prior period due to widespread statistically significant declines from the Mediterranean Sea eastward through the Fertile Crescent, southern Caspian Sea, and the Southwest Asian countries of Iran, Turkmenistan, and Afghanistan (Fig. 1a; Figs. S1a,b in the online supplemental material). Simultaneously, annual temperature increased by 1.2°C within this MESA region, with areas in Iran and Afghanistan warming by as much as 1.8°C (Fig. 1b; Figs. S1c,d).

In this article, we document and diagnose proximate causes of seasonal compound low-precipitation and high-temperature extremes in the recent compared to the prior period over this MESA region. Our goal is to identify physical factors related to

Supplemental information related to this paper is available at the Journals Online website: https://doi.org/10.1175/JCLI-D-23-0194.s1.

Corresponding author: Andrew Hoell, andrew.hoell@noaa.gov

DOI: 10.1175/JCLI-D-23-0194.1

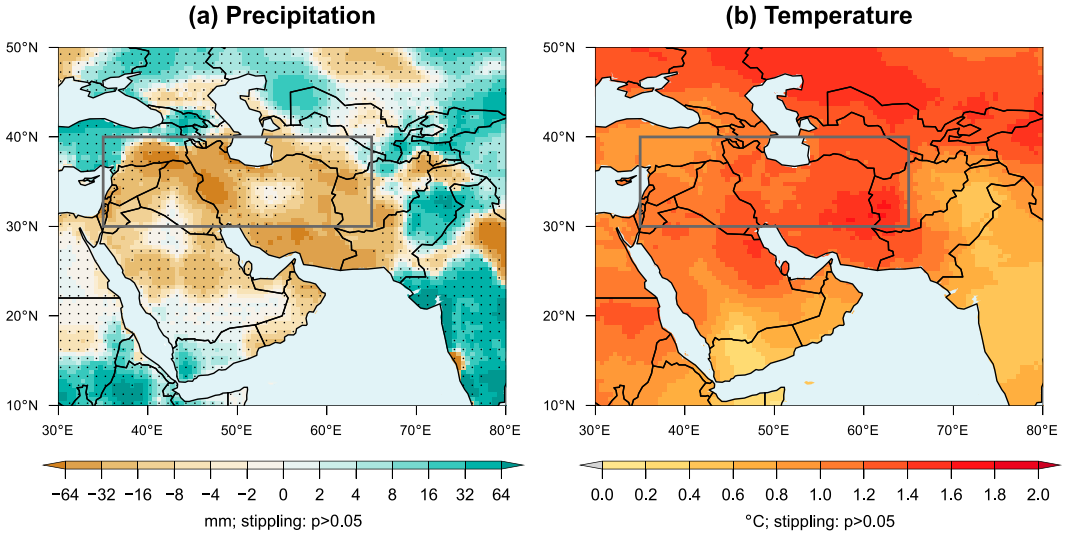

FIG. 1. Difference of observed (a) precipitation (mm) and (b) temperature (°C) estimates for September–August in a recent (1999–2022) compared to a prior (1951–98) period based on Climate Research Unit gridded datasets. Stippling indicates differences that are not statistically significant at $p < 0.05$ based on a bootstrapping approach described in section 2. The gray polygon outlines MESA.

compound drought and heat, potentially rendering future occurrences and their effects predictable in a MESA region that has been labeled a "prominent midlatitude" climate change hotspot (Giorgi 2006). We begin by documenting the preponderance of simultaneous low-precipitation and high-temperature seasons in the recent period over MESA during autumn (September–November), winter (December–February), spring (March–May), and summer (June–August), and attendant atmospheric circulation and sea surface temperatures (SSTs). We then use four transient coupled climate model ensembles to diagnose physical factors related to the observed compound drought and heat over MESA in each season, focusing on effects of SSTs consistent with La Niña and atmospheric forcing from greenhouse gases and aerosols. Our focus on SSTs is based on the oceanic origins of historical Southwest Asia precipitation (e.g., Hoell et al. 2017a), while our focus on the atmospheric forcing is based on increases in global temperature related to anthropogenic influences (e.g., Arias 2021, and references therein). The effects of SSTs and atmospheric forcing on seasonal compound drought and heat occurrences are diagnosed by comparing the frequency of these events related to ocean states in the transient climate model simulations where SSTs behave differently in each realization.

Our hypothesis concerning the effect of Indo-Pacific SST variability on low MESA precipitation in the recent period is based on the oceanic origins of historical Southwest Asia precipitation during the region's wet season that spans boreal autumn, winter, and spring (e.g., Hoell et al. 2017a). Links between Indo-Pacific SSTs and MESA precipitation have been principally investigated in terms of modes of organized climate variability, which include El Niño–Southern Oscillation (ENSO; e.g., Capotondi et al. 2015; Timmermann et al. 2018), the Indian Ocean dipole (IOD; e.g., Saji et al. 1999), and the Pacific decadal oscillation (PDO; e.g., Mantua et al. 1997). The SSTs related to these organized modes of climate variability are associated with anomalous atmospheric circulations over Asia, which in turn modify the behavior of eastward-moving storms (Kang et al. 2015; Abid et al. 2016) along the storm track across western Asia (e.g., Hoskins and Hodges 2019), which in turn leads to above- and below-average precipitation in MESA.

Regarding ENSO, its two opposing phases—El Niño and La Niña—are related to opposing precipitation anomalies over MESA during the region's wet season (e.g., Nazemosadat and Ghasemi 2004; Mariotti 2007; Hoell et al. 2013, 2015a, 2018; Cannon et al. 2017; Rana et al. 2017; Gerlitz et al. 2018, 2019; Barlow et al. 2021; Breeden et al. 2022). La Niña events, which are associated with cooler than average SSTs in the tropical east-central Pacific Ocean, are related to anomalous increases in tropical convection and precipitation in the west Pacific Ocean. This anomalous tropical convection is in turn associated with anomalous anticyclonic circulation over Southwest Asia, whose interaction with the mean flow leads to anomalous subsidence and attendant decreases in moisture flux and below-average MESA precipitation (e.g., Hoell et al. 2012, 2015). By contrast, El Niño events, which are associated with warmer than average SSTs in the tropical east-central Pacific Ocean, are related to anomalous decreases in tropical convection and precipitation in the west Pacific Ocean. This anomalous tropical convection is in turn associated with anomalous cyclonic circulation over Southwest Asia, whose interaction with the mean flow leads to anomalous ascent and attendant increases in moisture flux and above-average MESA precipitation (e.g., Hoell et al. 2012, 2015b). Also relevant in the context of climate change is the effect of increases in west Pacific SST anomalies during ENSO events on MESA precipitation (Barlow et al. 2002; Hoell and Funk 2013; Funk and Hoell 2015). Warmer west Pacific SST anomalies during La Niña events have been linked

TABLE 1. Precipitation and temperature estimates.

Dataset	Variable	Reference	Source
CRU: Climate Research Unit Time Series version 4.06	Precipitation	Harris et al. (2020)	https://crudata.uea.ac.uk/cru/data/hrg/
GPCC: Global Precipitation Climatology Centre version 6	Precipitation	Schneider et al. (2017)	https://psl.noaa.gov/data/gridded/data.gpcc.html
ERA5: European Centre for Medium-Range Weather Forecasts Reanalysis version 5	Precipitation	Hersbach et al. (2020)	https://cds.climate.copernicus.eu/cdsapp#!/dataset/reanalysis-era5-single-levels-monthly-means?tab=form
CRU	Temperature	Harris et al. (2020)	https://crudata.uea.ac.uk/cru/data/hrg/
Berkeley: Gridded Berkeley Earth Surface Temperatures	Temperature	Rohde and Hausfather (2020)	https://berkeley-earth-temperature.s3.us-west-1.amazonaws.com/Global/Gridded/Land_and_Ocean_LatLong1.nc
ERA5	Temperature	Hersbach et al. (2020)	https://cds.climate.copernicus.eu/cdsapp#!/dataset/reanalysis-era5-single-levels-monthly-means?tab=form

to a stronger anomalous atmospheric response over Asia, which in turn lead to comparably larger MESA precipitation deficits (Hoell et al. 2014a,b, 2017a) and the most intense historical droughts in the region (Barlow et al. 2016; Hoell et al. 2017b). Relatedly, long-lived patterns of Pacific SST anomalies averaged over given decades affect MESA precipitation (Hoell et al. 2015b, 2020). These SST patterns include features resembling the PDO, although the direct effect of the PDO is not apparent, given that the PDO is forced in part by sequences of El Niño or La Niña events on decadal time scales (Newman et al. 2016).

Regarding the IOD, its effect has been noted on MESA precipitation during autumn and early winter, given its seasonality (Saji et al. 1999; Xu et al. 2021). Hoell et al. (2015b) and Athar (2015) showed that Southwest Asia precipitation is related to an SST dipole across the equatorial Indian Ocean in November and December that resembles the IOD. The mechanisms responsible for this relationship include systematic atmospheric circulation anomalies that lead to anomalous moisture flux convergence and precipitation departures from average (e.g., Chakraborty et al. 2006; Abid et al. 2020). Abid et al. (2020) also noted that the effect of Indian Ocean SST dipoles can constructively or destructively interfere with the ENSO response. When ENSO and IOD work in tandem, the response over western Asia is stronger than if ENSO and IOD operate alone. Conversely, when ENSO and IOD are out of phase, the response over western Asia is weakened.

This study contributes to a growing volume of articles that focus on compound events, defined as simultaneous and/or sequential weather and climate events that lead to enhanced societal impacts compared to the effects from just a single event (Zscheischler et al. 2018, 2020; AghaKouchak et al. 2020; W. Zhang et al. 2021). Generalized compound event typologies have been proposed, which based on Zscheischler et al. (2020) include preconditioned, multivariate, temporally compounding, and spatially compounding types. Our focus on compound drought and heat falls into the category of multivariate events, which are projected to increase in a warming world and thus heighten effects on water resources for agriculture and consumption (e.g., Mukherjee and Mishra 2021; Tripathy et al. 2023). Tripathy et al. (2023) indicate that the easternmost area of our MESA region is among the areas of the world in which the frequency of compound drought and heat is projected to increase the most, which further motivates our study to explain these occurrences in the historical record.

This article is organized as follows. In section 2, we present the tools and methods used. In section 3, we document the seasonality of compound drought and heat since 1999 and attendant SSTs and atmospheric circulation. In section 4, we use climate model ensemble simulations to disentangle drivers of the recently observed compound precipitation and temperature extremes in MESA. In section 5, we summarize the principal conclusions and discuss their implications.

2. Tools and methods

a. *Tools*

We use observed estimates to document conditions relevant to seasonal precipitation and temperature in MESA during 1951–2022 to highlight the increases in compound drought and heat since 1999 (Table 1). Three observed precipitation estimates are used, given uncertainty arising from poor spatiotemporal sampling across the Middle East and Southwest Asia in the twentieth and twenty-first centuries (Hoell et al. 2015a, 2017a; McNally et al. 2022). Likewise, three observed temperature estimates are used. We also analyze observed SSTs based on the Extended Reconstructed SST version 5 (Huang et al. 2017) and atmospheric circulation based on ERA5 (Hersbach et al. 2020).

We use four transient coupled climate model ensembles to diagnose physical mechanisms related to compound drought and heat in MESA since 1999 (Table 2). Each model ensemble consists of many realizations from its namesake model that are forced by time-evolving conditions while aspects of internal variability differ among the realizations due to perturbations at initialization. The time-evolving drivers include natural and anthropogenic factors like greenhouse gases and aerosols (J. Zhang et al. 2021) while SSTs and the atmospheric circulation are internally simulated in each realization. The MPI, SPEAR, and CESM2 simulations are forced by historical conditions before 2015 and scenarios thereafter, with the former

TABLE 2. Model ensembles.

Model ensemble	References	Realizations	Historical period	Future period and forcing	Source
MPI: Max Planck Institute for Meteorology Earth System Model version 1.2	Mauritsen et al. (2019); Wieners et al. (2019a,b)	30	Before 2015 (Eyring et al. 2016)	SSP5-8.5 after 2015 (Eyring et al. 2016)	https://esgf-node.llnl.gov/projects/cmip6/
SPEAR: Seamless System for Prediction and Earth System Research Medium Configuration	Delworth et al. (2020)	30	Before 2015 (Eyring et al. 2016)	SSP5-8.5 after 2015 (Eyring et al. 2016)	https://www.gfdl.noaa.gov/spear_large_ensembles/
CESM2: Community Earth System Model version 2	Danabasoglu et al. (2020), Rodgers et al. (2021)	100	Before 2015 (Eyring et al. 2016)	SSP3-7.0 after 2015 (Eyring et al. 2016)	https://www.cesm.ucar.edu/projects/community-projects/LENS2/data-sets.html
CESM1: Community Earth System Model version 1	Kay et al. (2015)	40	Before 2005 (Taylor et al. 2012)	RCP8.5 after 2005 (Taylor et al. 2012)	https://www.cesm.ucar.edu/projects/community-projects/LENS/data-sets.html

two forced by SSP5-8.5 and the latter forced by SSP3-7.0. The CESM1 ensemble is forced by historical conditions before 2005 and the RCP8.5 scenario thereafter.

Monthly average conditions for 1951–2022 shown in Fig. 2 indicate that the climate models reproduce the observed mean precipitation and temperature annual cycles in MESA, although with biases that differ between models. We use the precipitation and temperature annual cycles to identify four 3-month seasons for study: autumn, winter, spring, and summer. As shown in Fig. 2a, the three observed precipitation estimates are similar and indicate month-over-month mean precipitation increases during autumn, consistently appreciable mean precipitation during winter, a mean precipitation increase in early spring that is followed by decreases through the end of this season, and a distinct dry season in summer. Mean precipitation biases across the annual cycle differ between the models. For example, the SPEAR model is consistently too wet, the MPI model is consistently too dry, and the CESM1 ensemble generally compares better with observed estimates, particularly during autumn and spring. As shown in Fig. 2b, the three observed temperature estimates and all but one model ensemble are similar, with a distinct cold season in winter, a distinct warm season in summer, and transition seasons in autumn and spring. A noteworthy outlier among the models is SPEAR, which has a pronounced cold bias during all months.

b. Methods

We define compound precipitation and temperature extremes as seasons in which the former quantity falls below −0.5 standardized departures (drought) and the latter quantity exceeds 0.5 standardized departures (heat) simultaneously. This definition is based on observed conditions documented in the following section and applied to the climate model simulations. Standardized precipitation and temperature departures, computed as a difference from the period average divided by the standard deviation, are based on 1951–2022. Precipitation and temperature anomalies are likewise computed as a difference from the 1951–2022 average. Regarding the labeling of years, each 3-month season takes the latter year of the September–August period in which it falls. For example, September 2020–August 2021 is labeled as 2021, and all 3-month seasons in that period are also labeled 2021: September 2020–November 2020, December 2020–February 2021, March 2021–May 2021, and June 2021–August 2021.

We use the oceanic Niño index (ONI) adopted by the NOAA Climate Prediction Center[1] to identify ENSO events. The ONI is defined as 3-month average SST anomalies in the Niño-3.4 region (5°S–5°N and 120°–170°W). Anomalies are based on averages computed from 30-yr periods around a target year and are updated every 5 years to isolate interannual variability in the midst of long-term warming.[2] For example, the ONI values for 1976–80 are based on averages during 1961–90. To calculate the ONI for years in which the base period would extend beyond recorded history (e.g., after 2010), a base period of 1991–2020 is used. La Niña events occur when the ONI falls below −0.5°C for five consecutive 3-month seasons, whereas El Niño events occur when the ONI exceeds 0.5°C for five consecutive 3-month seasons. ENSO neutral occurs when neither a La Niña nor an El Niño event is ongoing. Likewise, we compute seasonal SST anomalies in observed estimates and the model realizations similarly for consistency with the adopted ENSO definition.

Our analysis of the climate model ensembles involves identifying seasonal drought and heat since 1999 and examining whether systematic relationships exist between such compound events and physical features like SST anomalies and the atmospheric forcing by greenhouse gases and aerosols. The large sample size provided by each model ensemble offers an opportunity to demonstrate the robustness of relationships between compound drought and heat and physical features. Moreover,

[1] https://origin.cpc.ncep.noaa.gov/products/analysis_monitoring/ensostuff/ONI_v5.php.

[2] https://origin.cpc.ncep.noaa.gov/products/analysis_monitoring/ensostuff/ONI_change.shtml.

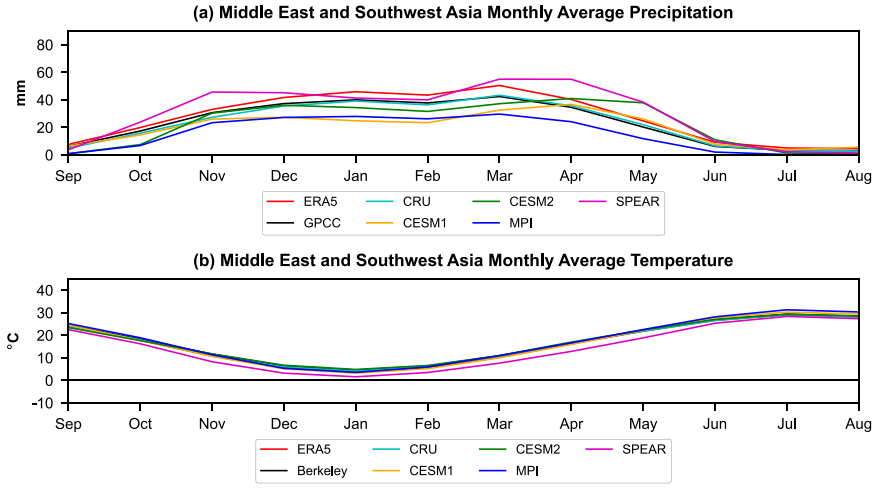

FIG. 2. Monthly average (a) precipitation (mm) and (b) temperature (°C) for the observed estimates and climate models indicated in the legends averaged over MESA during 1951–2022. The ensemble average of the model simulations is shown since there is little difference between realizations.

the analysis of four different models consisting of many realizations allows us to further demonstrate the robustness of results across models and to separate effects of inherent variability like ENSO from the externally forced variability due to human influences in each model ensemble (e.g., Tebaldi et al. 2011).

We diagnose the combined and individual effects of the atmospheric forcing by greenhouse gases and aerosols and La Niña on seasonal compound MESA drought and heat from three perspectives, each of which involves comparing different conditions in the climate models. We focus on La Niña due to its relationship with compound drought and heat indicated by analyses of observations and model simulations presented in the following. First, we diagnose the combined effect of atmospheric forcing and La Niña by comparing the frequency of compound drought and heat related to La Niña in the recent period to the same occurrences associated with non–La Niña (i.e., El Niño and ENSO neutral) in the prior period. Next, we diagnose the effect of atmospheric forcing by comparing the frequency of compound events in the recent period to the same occurrences in the prior period. Finally, we diagnose the effect of La Niña by comparing the frequency of compound events during La Niña in the recent period to the same occurrences associated with non–La Niña in the recent period.

We use bootstrapping to construct confidence intervals to assess statistical significance (Efron 1979). Random samples equal to the sample size of a target calculation are drawn with replacement from a population. The calculation is performed based on the random samples, and the process is repeated 10 000 times to construct a distribution from which the 95% confidence interval (2.5th and 97.5th percentile) is identified. If the target calculation exceeds or falls below the 95% confidence interval of the randomly sampled distribution, it is deemed to be statistically significant because there is less than a 5% chance of it occurring randomly.

We illustrate how bootstrapping is applied based on the following two examples. In the first, we seek to determine if a seven-value average of observed 250-hPa zonal wind anomalies in autumn is statistically different from the 1951–22 average at the 5% level ($p < 0.05$). Seven random samples are drawn with replacement from the entire population of 250-hPa zonal wind anomalies in 1951–2022, the seven samples are averaged, and the process is repeated 10 000 times. The seven-value average is compared to the distribution of 10 000 randomly sampled seven-value averages to determine if it exceeds the 95% confidence interval. In the second example, we seek to determine if the frequency of heat in autumn of the recent period is statistically different from the frequency of heat in autumn of the prior period based on the SPEAR climate model. The frequency of heat in autumn of the recent period is 75%, occurring in 543 of a possible 720 such seasons. The 720 random samples are drawn with replacement from the prior period of the SPEAR climate model, the frequency of heat is calculated, and the process is repeated 10 000 times. The frequency of heat in the recent period is compared to the distribution of 10 000 randomly sampled frequencies from the prior period to determine if it exceeds the 95% confidence interval.

3. Observed MESA compound drought and heat

We begin our presentation of results by documenting, characterizing, and diagnosing potential drivers for observed MESA compound drought and heat in the recent period during four 3-month seasons. Pronounced and persistent dryness prevailed in the recent compared to the prior period over MESA in winter and spring based on three different estimates of observed precipitation (Fig. 3). All three estimates are similar in terms of their magnitudes and interannual variability of anomalous precipitation in each of the four seasons when averaged over our MESA region, which indicates that the persistent dryness in the

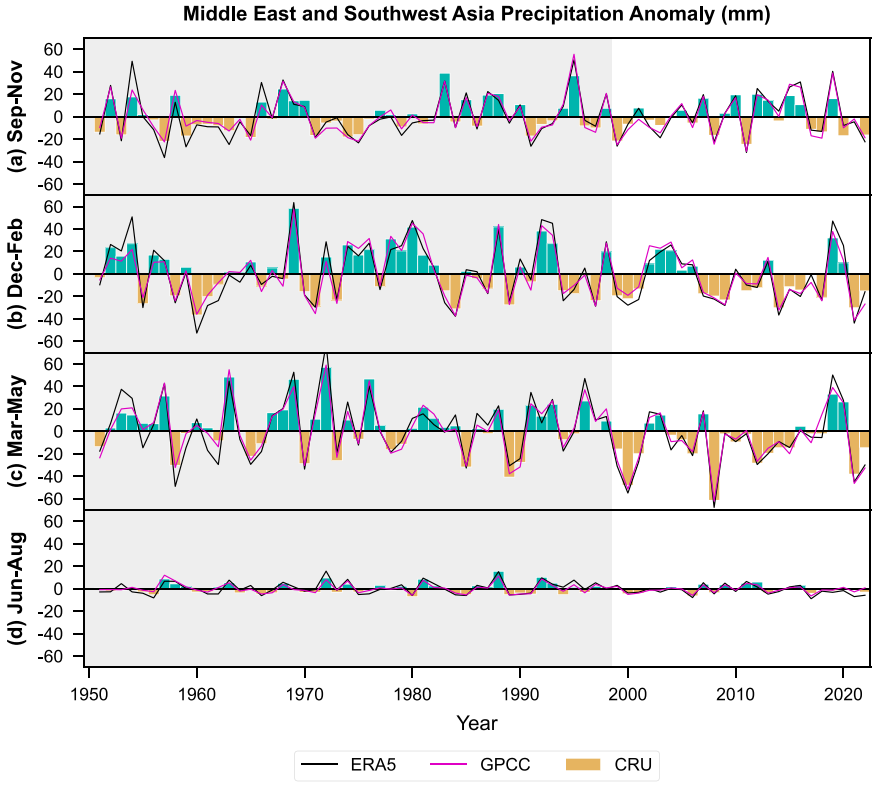

FIG. 3. Time series of MESA precipitation anomalies (mm) for (a) September–November, (b) December–February, (c) March–May, and (d) June–August based on CRU (bars), GPCC (magenta line), and ERA5 (black line). The prior period is shaded in gray.

recent period during the region's principal wet seasons is robust and not a feature of just a single dataset. We emphasize results from the CRU estimate, which serves as the basis for the analyses of observed conditions that follow, and note that the GPCC and ERA5 estimates indicate similar results.

The shift to dryness in winter and spring over MESA in the recent period is indicated by few examples of above-average precipitation and many examples of below-average precipitation, some of which rival the lowest such precipitation seasons during 1951–2022 (Figs. 3b,c). In winter, above-average precipitation was observed in eight of 23 seasons in the recent period, with only one season ranking in the top 10 wettest seasons in the entire period of record (Fig. 3b). Persistent year-over-year wintertime dryness was also observed, whereby below-average precipitation prevailed for six consecutive seasons (2007–12) and five consecutive seasons (2014–18). In spring, similar precipitation features compared to winter are apparent (Fig. 3c). Above-average precipitation was observed in just six of the 23 seasons in the recent period, and none of those six seasons ranked among the top five wettest in 1951–2022. Moreover, three of the four driest spring seasons in the entire period of record occurred in the recent climate, precipitation was below average in eight consecutive spring seasons (2008–15), and there were three separate occurrences in which spring precipitation was below average for at least three consecutive years. Less precipitation was observed in autumn and summer compared to winter and spring over MESA, with the latter season contributing very little to annual precipitation (Fig. 2). In autumn of the recent period, a shift to dryness over MESA was not observed like in winter and spring. There was nearly an equal frequency of below-average (12) and above-average (10) precipitation seasons, with two other seasons virtually indistinguishable from average (Fig. 3a). However, the driest autumn in MESA, as well as three of the top five driest such seasons, was observed in the recent period.

Likewise, pronounced and persistent above-average temperatures prevailed in the recent period over MESA due to a shift to warmer temperatures in all seasons (Fig. 4). All three observed estimates indicate similar magnitudes and interannual variability of anomalous seasonal temperatures when averaged over the MESA region, which demonstrates the robustness of the identified features. In the recent period, there were few examples of below-average temperatures in autumn (2), winter (6), spring (1), and summer (0). Not only were above-average temperatures persistent in the recent period, but an overwhelming number of the warmest seasons compared to the entire period of record were observed since 1999. Combining March–May and June–August to measure the warm half of the year, temperatures were above average for this 6-month stretch since the late 1990s. While winters since 1999 saw the

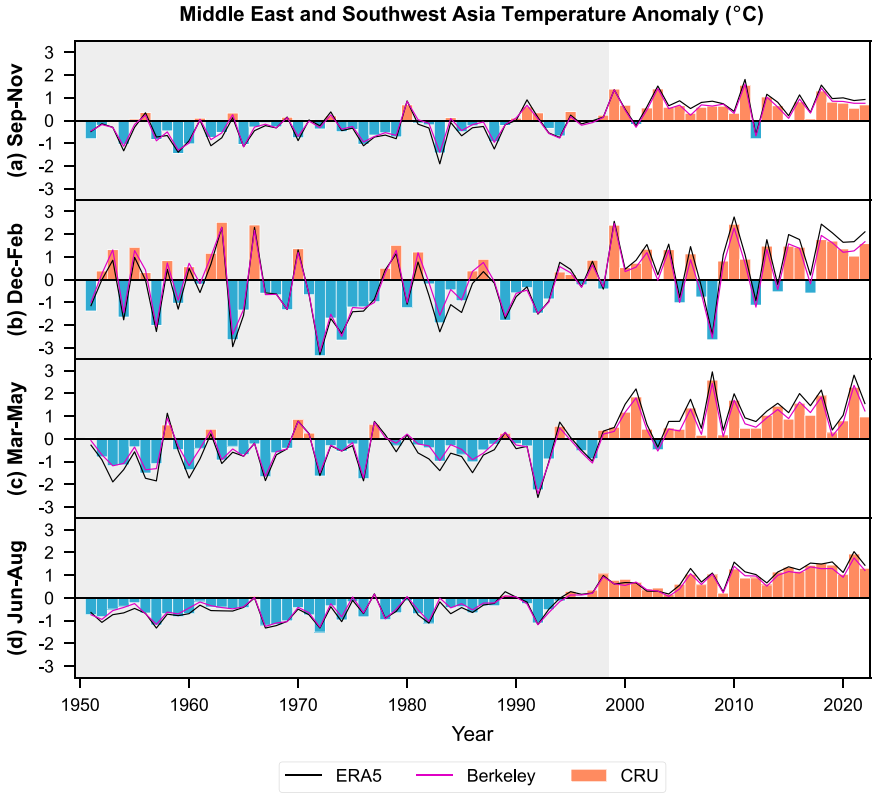

FIG. 4. Time series of MESA temperature anomalies (°C) for (a) September–November, (b) December–February, (c) March–May, and (d) June–August based on CRU (bars), Berkeley (magenta line), and ERA5 (black line). The prior period is shaded in gray.

greatest frequency of below-average temperatures compared to the other three seasons, anomalous temperatures in each of the last five in 1951–2022 were above 0.9°C.

The prevalence of below-average precipitation and above-average temperatures over MESA since 1999 led to a preponderance of compound drought and heat extremes in all seasons in the recent compared to the prior period (Fig. 5). Scatter relationships between temperature and precipitation indicate that in autumn, seven compound drought and heat extremes were observed in the recent period compared to just one in the prior period. In winter, nine compound extremes were observed in the recent period compared to six in the prior period. In spring, 10 compound extremes were observed in the recent period compared to two in the prior period. In summer, seven compound extremes were observed in the recent period and none in the prior period. Although MESA compound drought and heat was more frequent in the recent compared to the prior period during all seasons, the way in which observed seasonal precipitation and temperature covaried to produce these compound extremes differs between them (Fig. 5). In spring, the correlation between precipitation and temperature is -0.59 ($p < 0.001$), so it follows that the warmest and driest seasons tended to occur simultaneously, 80% of which were found in the recent period (Fig. 5c). Likewise, the coolest and wettest spring seasons also tended to occur simultaneously, all of which were found in the prior period. In autumn (Fig. 5a) and winter (Fig. 5b), the correlations between precipitation and temperature are not statistically significant, and the relationship between the two quantities suggests that compound heat and drought would occur by chance. However, this is not the case, particularly in autumn, based on the preponderance of compound events in the recent compared to the prior period. A key reason for the increase in the prevalence of compound drought and heat in autumn and winter is likely due to warmer temperatures in the recent period (Fig. 4), which leads to above-average temperatures in what would otherwise just be a below-average precipitation and near-average temperature season in the prior period. It is important to note that June–August is the dry season in MESA (Fig. 2) and heat extremes alone in this season are of primary importance to societal impacts in the region compared to compound heat and drought.

Seasonal MESA compound drought and heat in the recent period was related to a northward shift of the jet stream along which storms move through western Asia (Fig. 6) and corresponding decreases in the convergence of vertically integrated moisture flux in MESA (Fig. S2). The jet stream across western Asia, indicated by the area of maximum average 250-hPa zonal winds during 1951–2022, enables precipitation-bearing storms to move through the region in the autumn, winter, and spring precipitation seasons. Compound drought and heat in these seasons are related to decreases in the magnitude of 250-hPa zonal winds in the area of the climatological

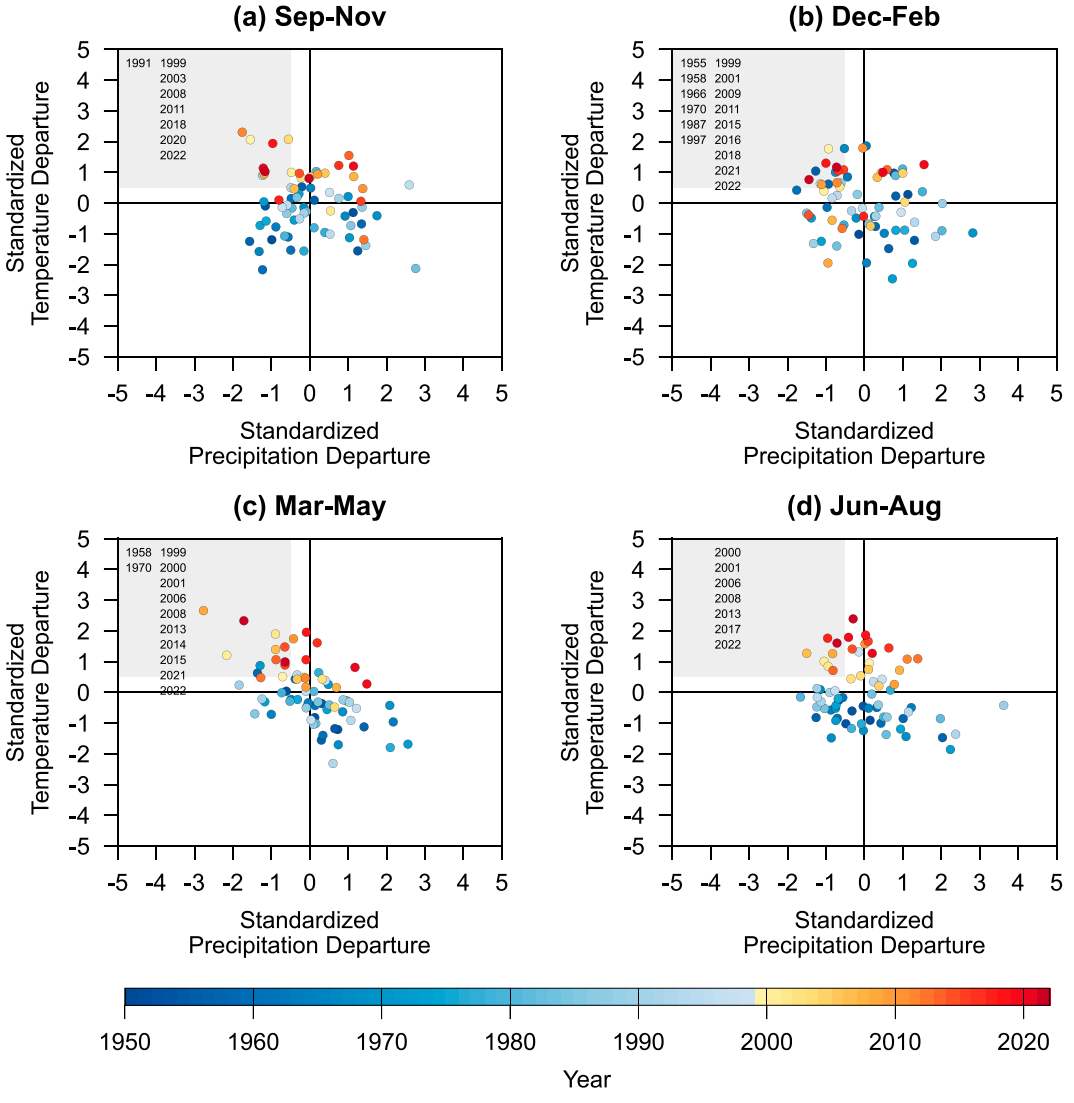

FIG. 5. Scatter relationship of MESA standardized temperature and precipitation departures based on CRU with shading indicating years from 1951 to 2022 during (a) September–November, (b) December–February, (c) March–May, and (d) June–August. Gray shading indicates the area in which precipitation is less than −0.5 standardized departures and temperature greater than 0.5 standardized departures. The years in which compound drought and heat were observed are noted.

maximum and increases in the magnitude of the jet-level winds to the north, which is indicative of a northward displacement of the jet stream and storm track. When viewed from the perspective of wind vectors, the north–south orientation of zonal wind anomalies at 250 hPa appears as an anomalous anticyclonic circulation in western Asia (not shown). Corresponding decreases in vertically integrated moisture flux convergence are also noted in MESA during the autumn, winter, and spring precipitation seasons related to compound drought and heat (Fig. S2). The anomalous vertically integrated moisture flux is from the northeast in MESA, which is not an abundant moisture source, and the anomalous vertically integrated moisture flux increases in magnitude away from MESA, contributing to increases in precipitation-reducing anomalous divergence.

Observed MESA compound drought and heat in the recent period was related to SST anomalies that closely resemble La Niña, with below-average SSTs in the central and eastern tropical Pacific Ocean and above-average SSTs in the western Pacific Ocean (Fig. 7). Seasonal differences in the Pacific Ocean SST pattern include a progression in the area of maximum below-average SST anomalies from the east to central Pacific Ocean from autumn through winter, spring, and summer. The SST anomalies consistent with La Niña in the central and west Pacific Ocean are generally statistically significant at the 95% level despite this being a strict threshold

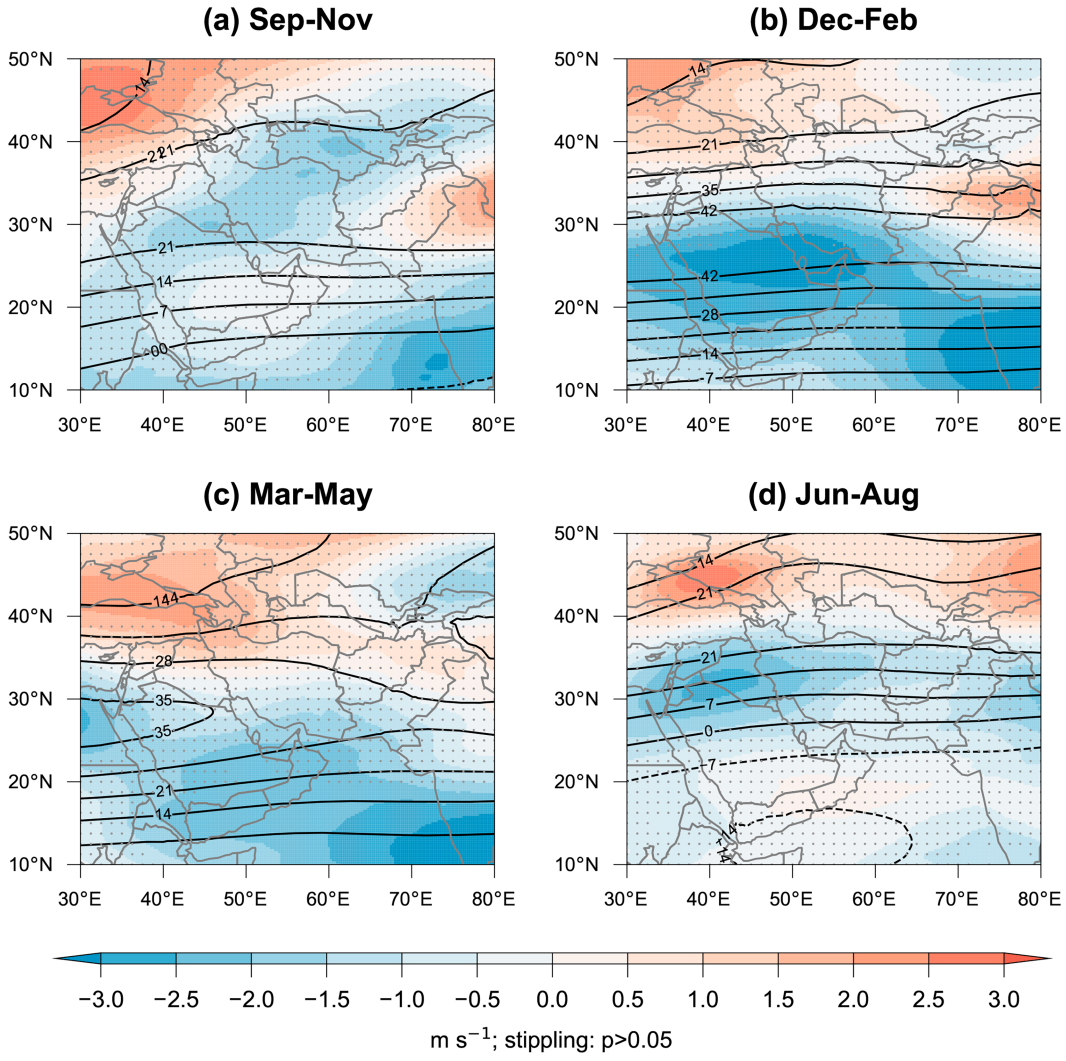

FIG. 6. Average observed 250-hPa zonal wind anomaly (shading; m s^{-1}) during MESA compound drought and heat events in the recent period and average 250-hPa zonal wind during 1951–2022 (contour; m s^{-1}) for (a) September–November, (b) December–February, (c) March–May, and (d) June–August. Stippling indicates zonal wind anomalies that are not statistically significant at $p < 0.05$.

given the number of events considered in the composite (Fig. 5). SSTs elsewhere in the global oceans related to MESA compound drought and heat since 1999 are generally not found to be statistically significant. These seasonal SST composites do not convincingly indicate a pattern consistent with the IOD, namely, an SST dipole between the western and eastern Indian Ocean along the equator.

4. MESA compound drought and heat in climate models

We continue our presentation of results by examining physical features related to compound drought and heat in MESA using the four transient coupled climate model ensembles. We do so to test the robustness of the features identified in observed estimates and to diagnose the effects of SSTs and atmospheric forcing on compound drought and heat in MESA. We begin by identifying local atmospheric circulation and global SSTs related to regional compound drought and heat in the climate models. We then use these tools to diagnose the individual and combined effects of atmospheric forcing and La Niña on seasonal compound MESA drought and heat by comparing different conditions in the climate models based on the three perspectives described in the methods section (section 2b).

Like observed estimates shown in Fig. 6, MESA compound drought and heat in the recent period from the climate models is related to a northward shift of the jet stream along which precipitation-bearing weather systems move across the Middle East and southwest Asia during the autumn, winter, and spring wet seasons (Fig. 8). All models indicate a decrease in the magnitude of 250-hPa zonal winds across western Asia between 25° and 35°N and an increase in the jet-level winds to

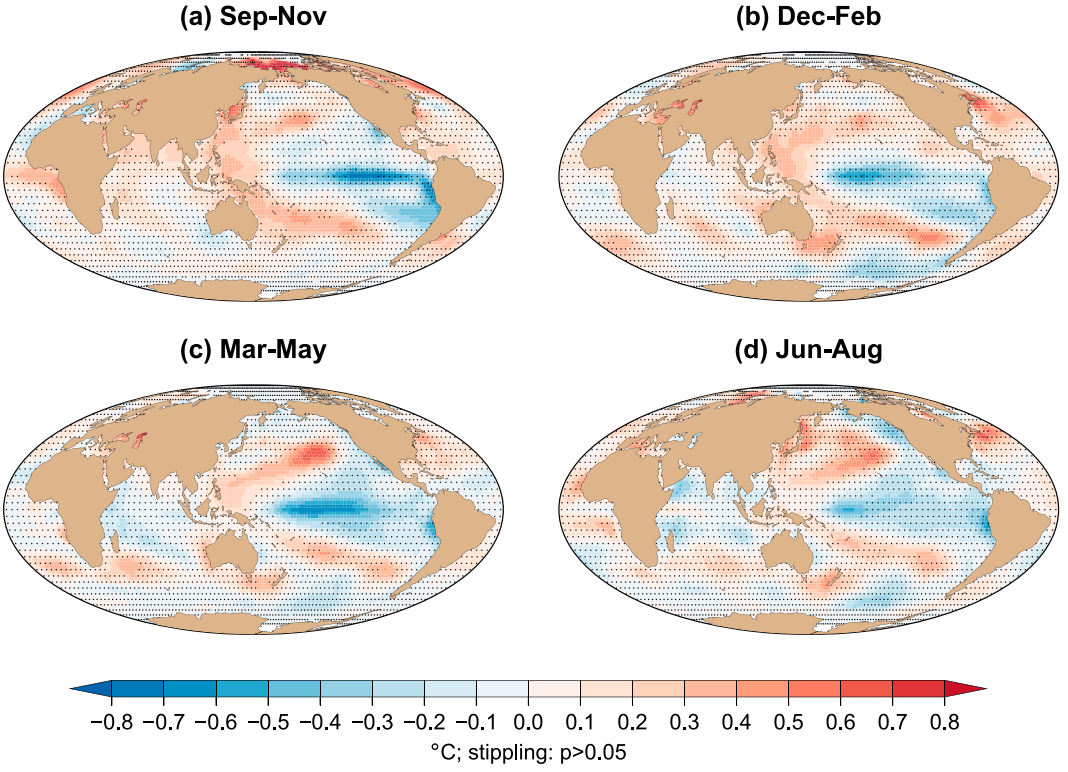

FIG. 7. Average observed SST anomaly (°C) during MESA compound drought and heat events in the recent period for (a) September–November, (b) December–February, (c) March–May, and (d) June–August. Stippling indicates SST anomalies that are not statistically significant at $p < 0.05$.

the north related to MESA compound drought and heat. These features suggest a northward displacement of the jet stream and storm track that disrupts precipitation-bearing storms in western Asia, which leads to below-average precipitation during the MESA wet seasons. When viewed from the perspective of wind vectors, the north–south orientation of zonal wind anomalies at 250 hPa in the climate models appears as an anomalous anticyclonic circulation in western Asia, like observed estimates (not shown). It is also important to highlight the strong consensus in the pattern and magnitude of 250-hPa wind anomalies related to compound drought and heat in MESA for each wet season across the four climate models. Note that the mean 250-hPa zonal winds are not shown in Fig. 8 like they are in Fig. 6 to highlight anomalies from the four climate models during the four seasons.

Like observed estimates shown in Fig. 7, MESA compound drought and heat in the recent period from the climate models is related to global SST anomalies during all seasons (Fig. 9). The SST anomalies across seasons and models are generalizable, characterized principally by patterns that resemble La Niña, although it is important to note that details of the SST anomaly patterns and their statistical significance differ somewhat by season and model. Differences between seasons suggest potential varying sensitivity of MESA drought and heat to SST patterns between different parts of the year. Differences in SST patterns between climate models highlight uncertainties in the true relationships due to potential model biases, which indicates the benefits of a multimodel approach of such a study to better appreciate the existence of biases.

In autumn (Fig. 9, left column), and consistent with observed estimates (Fig. 7a), all climate models indicate a prominent relationship between MESA compound drought and heat and La Niña, as indicated by statistically significant below-average SST anomalies in the central and eastern tropical Pacific Ocean and above-average SST anomalies in the western tropical Pacific Ocean. The SST anomalies in the Pacific Ocean differ somewhat between the four climate models: the CESM models indicate stronger relationships and below-average SST anomalies that are farther to the east, while the MPI model indicates weaker relationships and below-average SST anomalies farther to the west. SST anomalies related to MESA compound drought and heat also differ in the Indian Ocean, with some models displaying a pattern that resembles a negative IOD (Fig. 9, left column). This suggests uncertainty regarding the effect of the IOD on MESA compound drought and heat, especially considering that an IOD pattern is not present in the observed perspective shown in Fig. 7a. The CESM1 and SPEAR models prominently display statistically significant SSTs consistent with a negative IOD, with below-average SST in the western Indian Ocean and above-average SST in the eastern Indian Ocean. There is a suggestion of such a pattern in the CESM2 ensemble, though

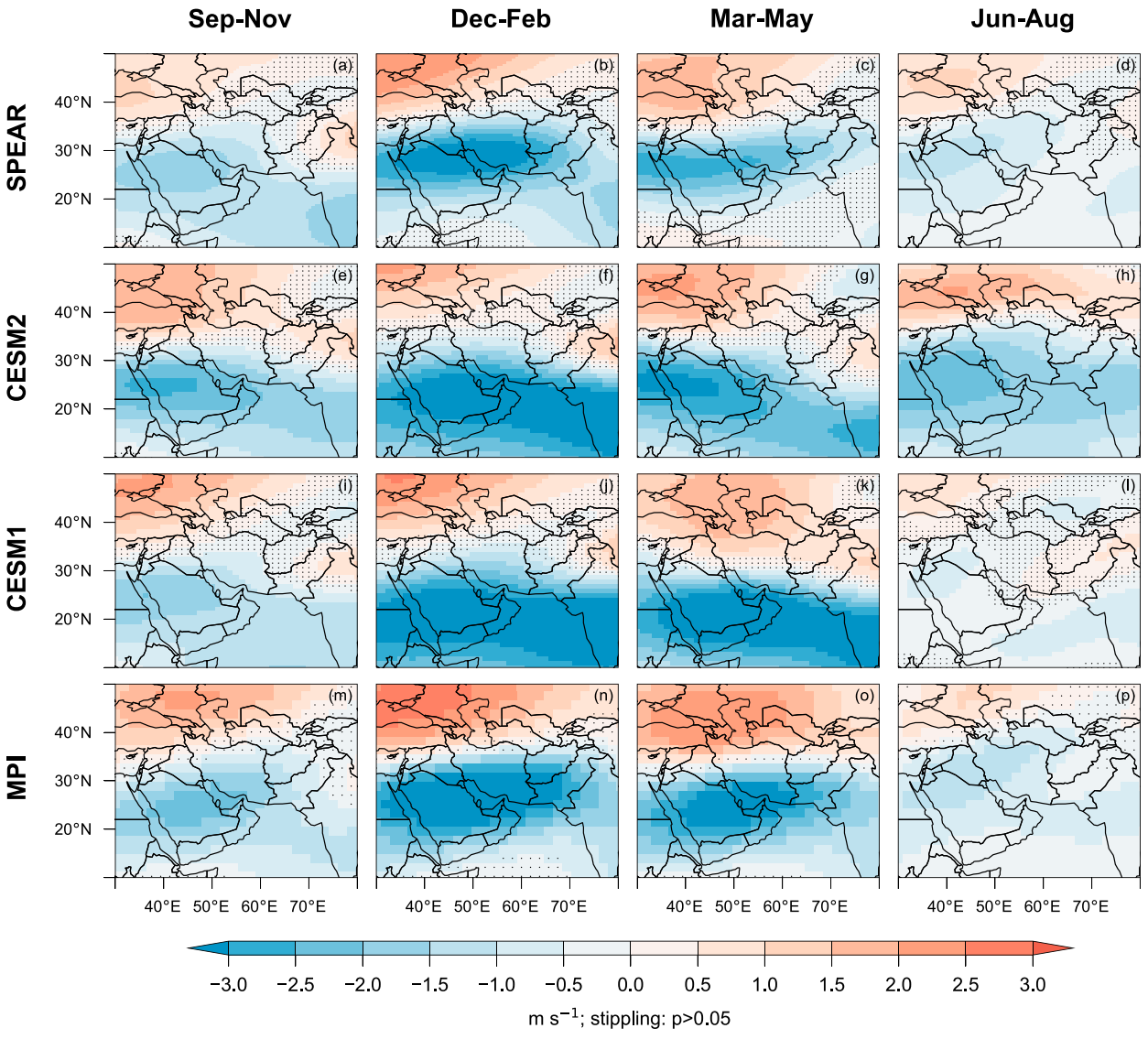

FIG. 8. Average 250-hPa zonal wind anomaly (m s^{-1}) during MESA compound drought and heat events in the recent period for (a)–(d) SPEAR, (e)–(h) CESM2, (i)–(l) CESM1, and (m)–(p) MPI during (left) September–November, (center left) December–February, (center right) March–May, and (right) June–August. Stippling indicates zonal wind anomalies that are not statistically significant at $p < 0.05$. All model ensemble members are included in these calculations.

not as prominent in terms of the magnitude of the SSTs and their statistical significance. No such IOD pattern is indicated by the MPI model.

In winter (Fig. 9, center-left column), intermodel differences regarding SST relationships with MESA compound drought and heat are noted, although all provide at least some suggestion of a pattern in the tropical Pacific Ocean that resembles La Niña, which is consistent with observed estimates (Fig. 7b). The CESM family of climate models indicates very pronounced statistically significant SST patterns consistent with La Niña, as indicated by below-average SST in the central and eastern Pacific Ocean and above-average SST in the western Pacific Ocean. The SPEAR and MPI models indicate much more subtle SST patterns consistent with La Niña, as indicated by the central and western contrast of SST anomalies in the tropical Pacific Ocean. These SST patterns indicate statistically significant anomalies in the western Pacific Ocean from both models, while the SPEAR model indicates statistically significant anomalies in the central Pacific Ocean. Elsewhere in the global ocean during winter, no consistent SST anomaly patterns are found between the four climate model ensembles.

In spring (Fig. 9, center-right column), intermodel differences regarding SST relationships with MESA compound drought and heat are also noted, which resemble the same patterns found in winter. These patterns, consistent with La Niña, in which below-average SST anomalies are found in the tropical central Pacific Ocean and above-average SST anomalies are found in the western Pacific, are compatible with

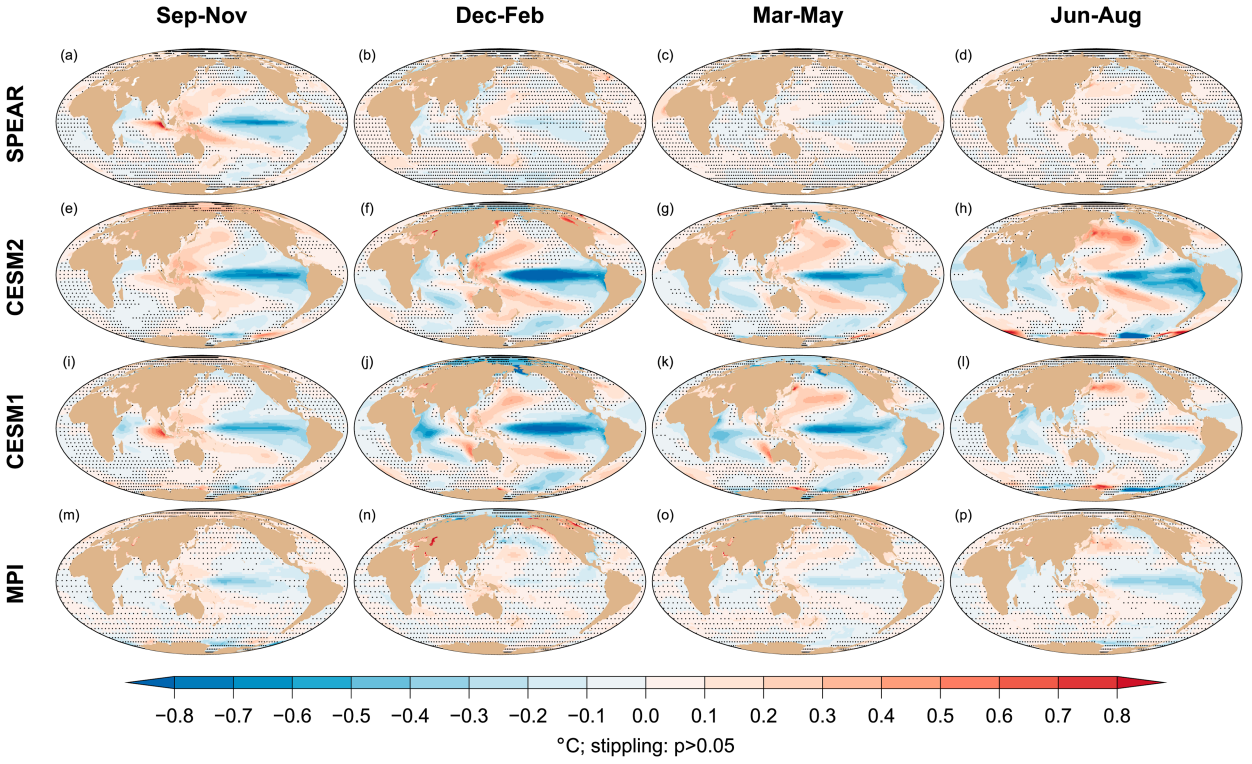

FIG. 9. Average SST anomaly (°C) during MESA compound drought and heat events in the recent period for (a)–(d) SPEAR, (e)–(h) CESM2, (i)–(l) CESM1, and (m)–(p) MPI during (left) September–November, (center left) December–February, (center right) March–May, and (right) June–August. Stippling indicates SST anomalies that are not statistically significant at $p < 0.05$. All model ensemble members are included in these calculations.

observed estimates shown in Fig. 7c. Once again, the CESM models indicate very pronounced statistically significant SST patterns consistent with La Niña, while the SPEAR and MPI models indicate much more subtle patterns. Finally, in summer (Fig. 9, right column), intermodel differences regarding SST relationships with MESA compound drought and heat are found, likely due to the seasonality of precipitation (Fig. 2). Three of the four models indicate an SST pattern related to La Niña, although differences are found even between these three models (SPEAR, CESM2, and MPI) in terms of the magnitude of the composite anomalies and their statistical significance.

We now turn our attention to diagnosing the combined and individual effects of La Niña and the atmospheric forcing by greenhouse gases and aerosols on seasonal MESA compound drought and heat. We do so by comparing conditions in the climate models controlled by La Niña in the recent and prior periods. These comparisons, shown in Figs. 10–12, involve scatter relationships between MESA temperature and precipitation standardized departures from each of the four climate models, with probability density functions (PDFs) indicating the distributions of the two quantities. Also shown are the frequency of compound drought and heat, drought, and heat, and whether the frequencies are significantly different at the 95% level compared to the entire 1951–2022 period.

A comparison of La Niña in the recent period to non–La Niña in the prior period shown in Fig. 10 indicates that the combined effect of La Niña and atmospheric forcing by greenhouse gases and aerosols leads to lower precipitation, higher temperatures, and therefore statistically significant increases in the frequency of drought, heat, and their simultaneous occurrences in MESA. These results provide further evidence for the combined effects of La Niña and anthropogenic influences on MESA compound drought and heat since 1999 identified in observed estimates (Figs. 3, 4, 5, and 7). Results are consistent across models and seasons, whereby a shift to lower precipitation and higher temperatures is found during autumn, winter, and spring with few exceptions. Impressively, compound drought and heat related to La Niña in the recent period occur 32%–44% of the time, which is far greater than these occurrences during 1951–2022 unconditioned on La Niña, which occur about 10%–20% of the time. Concerning temperature, different magnitudes of seasonal warming between the prior and recent periods are noted in the climate models, the largest of which is found in summer (2 standardized departures), with more modest warming in the other three seasons (1–1.5 standardized departures). Warming is largest in the SPEAR model and comparably more modest in the CESM models. Concerning precipitation, seasonal decreases related to La Niña in the recent period compared to non–La Niña in the prior period are notable and differ somewhat by season and

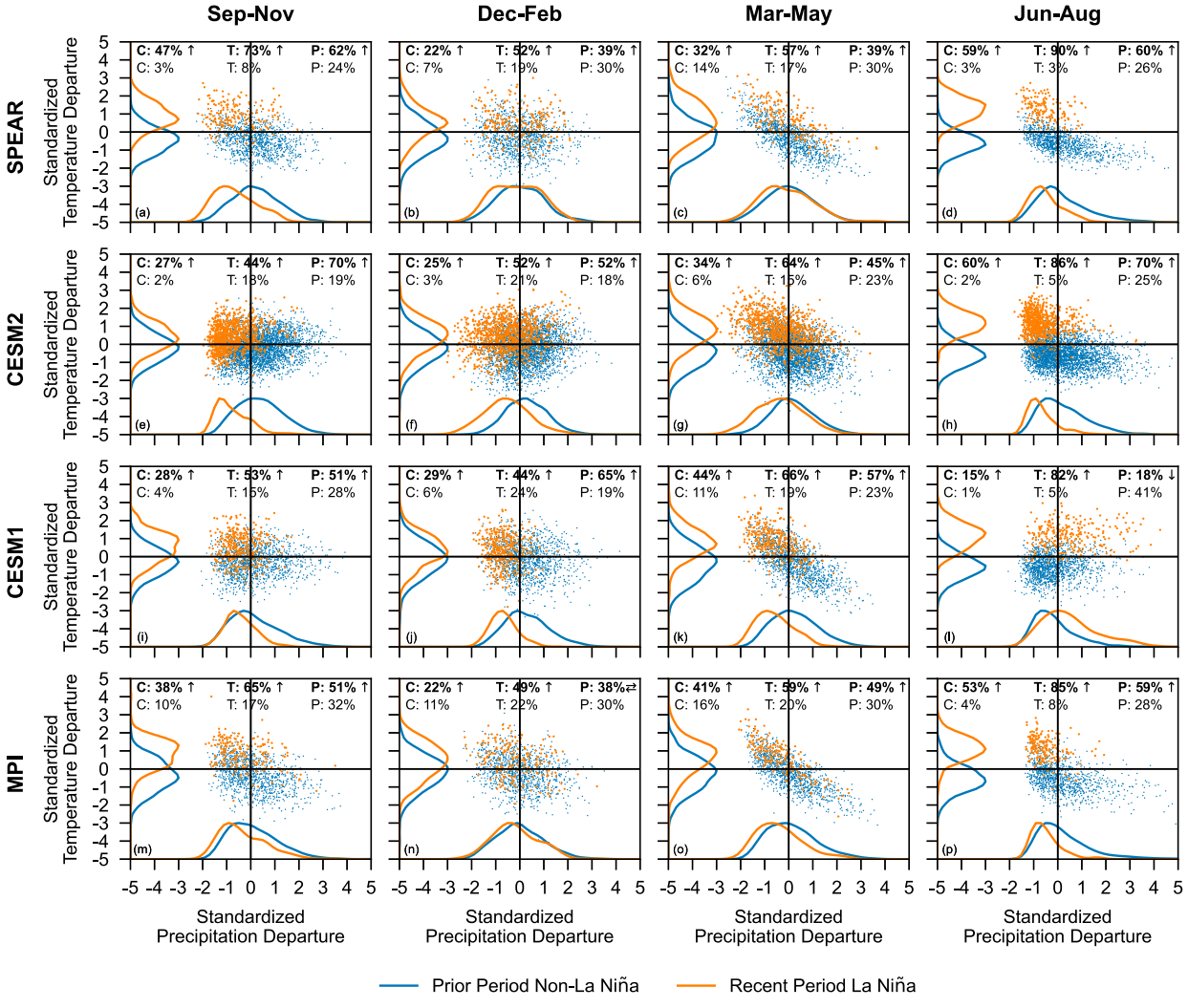

FIG. 10. For La Niña in the recent period (orange) and non–La Niña in the prior period (blue), scatter relationship of MESA standardized temperature and precipitation departures for (a)–(d) SPEAR, (e)–(h) CESM2, (i)–(l) CESM1, and (m)–(p) MPI during (left) September–November, (center left) December–February, (center right) March–May, and (right) June–August. Also shown are temperature (vertical axis) and precipitation (horizontal axis) PDFs smoothed by a nonparametric kernel density estimator. Labels along the top of the scatterplots indicate the occurrence likelihood of a compound drought and heat event (C), a heat event only (T), and a drought event only (P). Bold labels indicate conditions shown in orange, here La Niña in the recent period, and labels in normal font indicate conditions shown in blue, here non–La Niña in the prior period. An upward arrow indicates a statistically significant increase, a downward arrow indicates a statistically significant decrease, and two horizontal arrows indicate that the frequency does not indicate a statistically significant difference. All model ensemble members are included in these calculations.

model. The largest decreases are found in spring and autumn and in the CESM models, consistent with the SST composites shown in Fig. 9.

A comparison of recent and prior periods unconditioned on ENSO shown in Fig. 11 indicates that differences in the atmospheric forcing between the two epochs are related to statistically significant increases in the frequency of MESA heat during all seasons that is unanimous across the climate models, but there is little indication of statistically significant changes in the frequency of MESA drought. These results provide evidence for the effect of greenhouse gases and aerosols on increases in temperature yet little effect on precipitation. Temperature increases are generally consistent with those found in the same comparison of recent La Niña and prior non–La Niña (cf. Figs. 11 and 10), which suggests that atmospheric forcing plays the primary role in modulating temperatures. Temperature increases lead to statistically significant increases in MESA heat, which in turn leads to statistically significant increases in the frequency of a compound extreme during all seasons because of drastic shifts in the distributions of regional temperatures to warmer conditions of at least one standard deviation. The effect of this is for warmer temperatures in

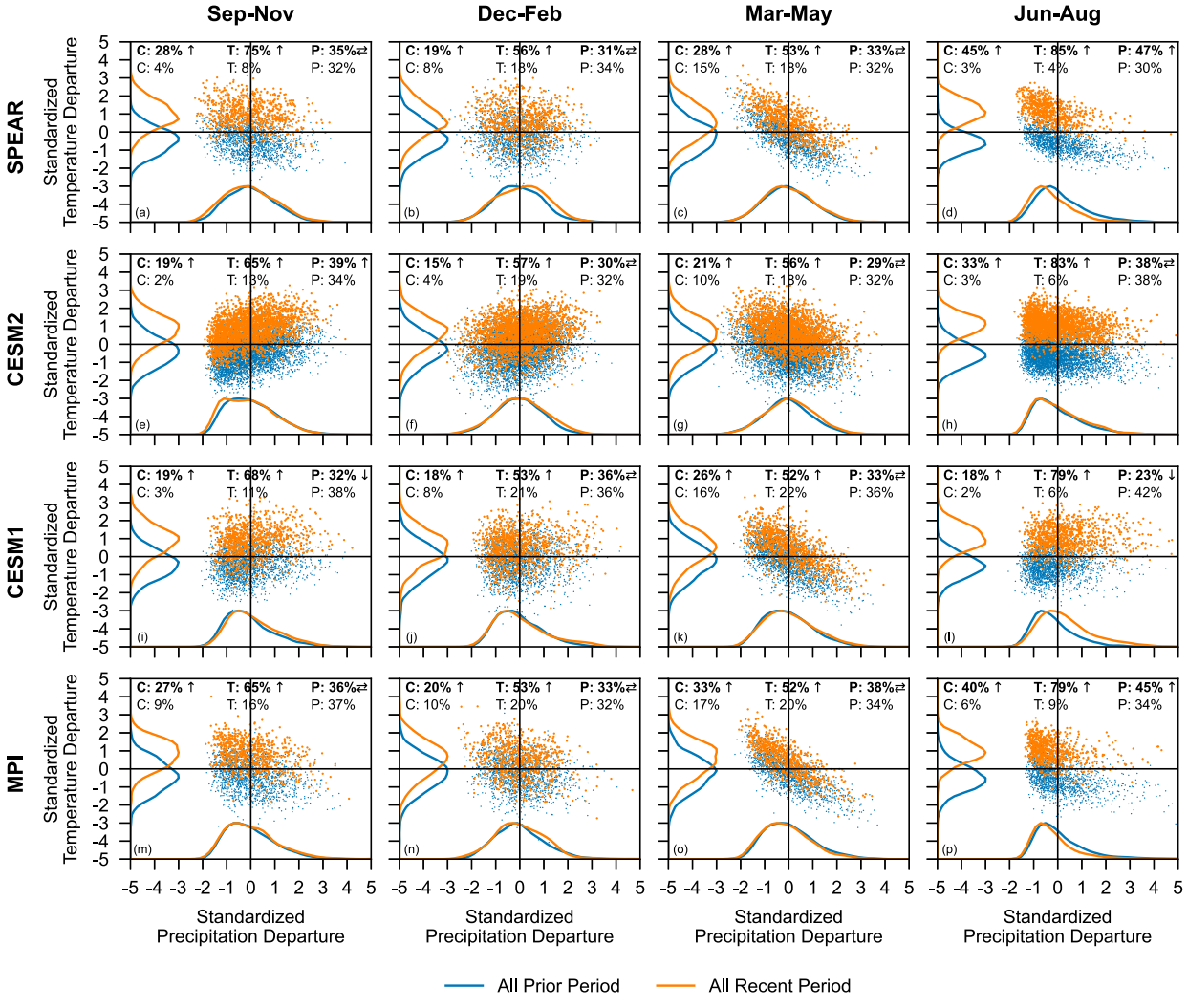

FIG. 11. As in Fig. 10, but for the recent period (orange) and prior period (blue).

a recent climate in what would otherwise be a below-average precipitation and near-average temperature season in the prior period, thereby elevating the likelihood of a compound drought and heat season.

A comparison of La Niña and non–La Niña both in the recent period shown in Fig. 12 indicates that La Niña is related to lower precipitation during the MESA wet seasons in the climate models and attendant increases in the likelihood of drought. This comparison also reveals that La Niña is not related to differences in temperature that are consistent across climate models and seasons. Precipitation decreases are generally consistent with those found in the same comparison of recent and prior periods conditioned on ENSO (cf. Figs. 12 and 10), which suggests that La Niña plays the primary role in modulating precipitation during compound drought and heat extremes. Precipitation decreases related to La Niña lead to statistically significant increases in the frequency of MESA drought with few exceptions, which generally lead to statistically significant increases in the frequency of a compound drought and heat season. These results are also supported by a comparison of La Niña in the recent and prior periods shown in Fig. S3, which indicate increases in heat between the two periods, but little indication of systematic changes in drought between the two periods related to La Niña.

5. Summary, conclusions, and discussion

Motivated by the conflict, migration, and water shortages associated with compound drought and heat since 1999 over a Middle East and Southwest Asia (MESA) area spanning from the eastern Mediterranean to western Afghanistan between 30° and 40°N, we documented and diagnosed proximate causes for increases in simultaneous seasonal low-precipitation and high-temperature extremes in a recent (1999–2022) compared to a prior (1951–98) period in this region. In terms of documentation, we detailed the preponderance of simultaneous low-precipitation and high-temperature seasons in the recent period and characterized the attendant atmospheric circulation and

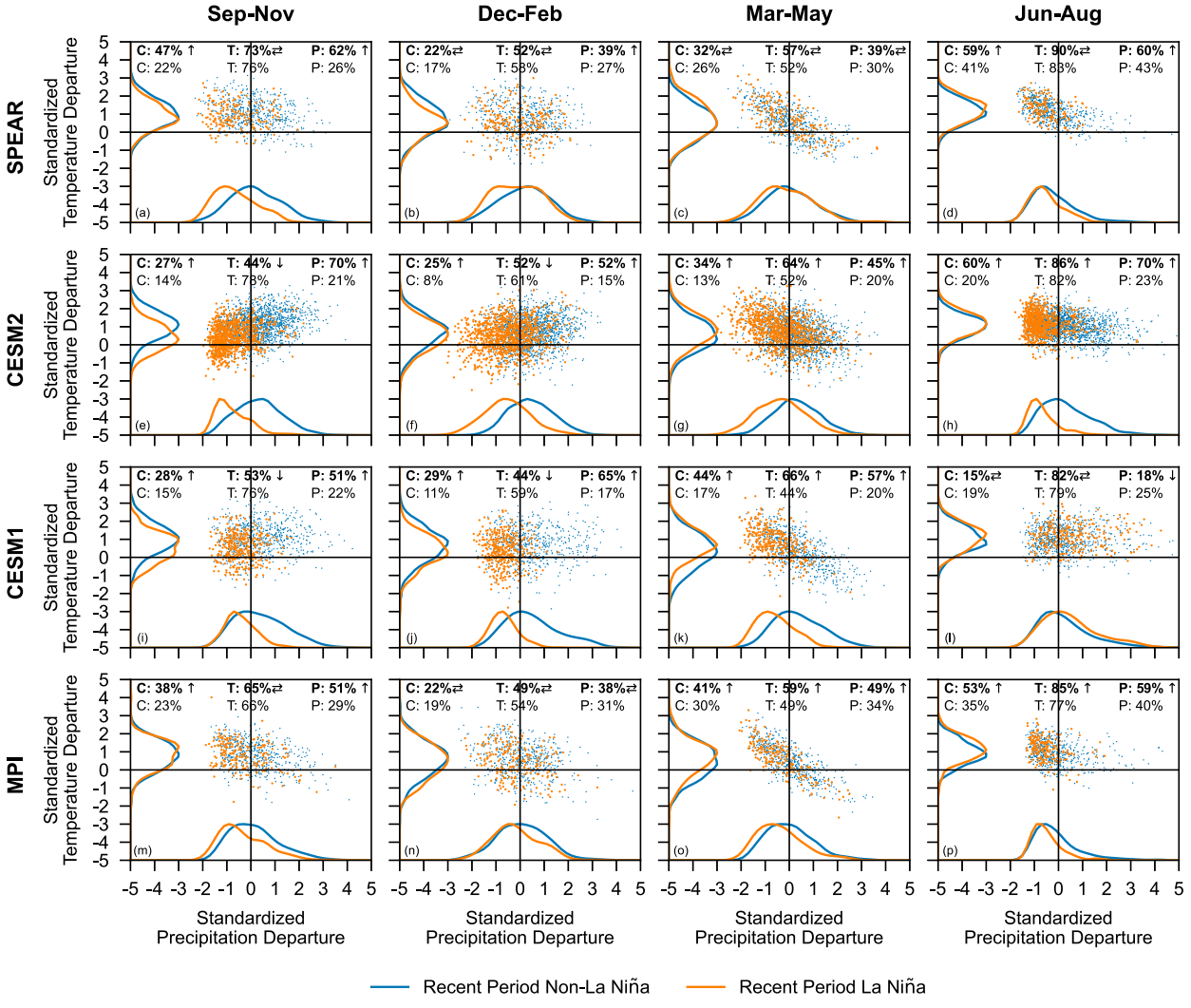

FIG. 12. As in Fig. 10, but for La Niña in the recent period (orange) and non–La Niña in the recent period (blue).

SSTs. In terms of proximate causes, we used coupled climate model ensembles to diagnose the effect of La Niña and atmospheric forcing from greenhouse gases and aerosols on simultaneous MESA drought and heat in autumn, winter, spring, and summer, which may be used to provide practical forecast skill for future compound events.

MESA compound drought and heat were a frequent occurrence in the recent compared to the prior period in all seasons, where drought was defined as precipitation falling below −0.5 standardized departures and heat defined as temperature exceeding 0.5 standardized departures. For example, in autumn, seven compound extremes were observed in the recent period compared to one in the prior period, while in spring, 10 compound extremes were observed in the recent period compared to two in the prior period. The preponderance of compound drought and heat in the recent period was caused by the prevalence of both below-average precipitation and above-average temperatures since 1999. Concerning precipitation, many examples of drought were noted in all seasons since 1999, with dryness often persisting for many consecutive years. Concerning temperatures, a pronounced shift to above-average temperatures was noted in MESA during all seasons, as indicated by few examples of below-average temperatures in any season. For example, only a single season with below-average temperatures was observed in both autumn and spring in MESA since 1999.

Attendant atmospheric circulation and SSTs related to seasonal compound MESA drought and heat reveal a northward shift in the storm track and related decreases in the convergence of vertically integrated moisture flux in western Asia, as well as oceanic conditions accordant with La Niña. A northward displacement of the storm track is indicated in observations and climate models via a decrease in 250-hPa zonal wind over MESA and an increase in zonal winds to the north, which suggests a disruption of the typical movement of precipitation-bearing storms that leads to below-average precipitation in western Asia. SSTs consistent with La Niña, characterized by below-average SSTs in

the tropical central Pacific and above-average SSTs in the western Pacific, were a prominent feature related to compound MESA drought and heat in observations and the climate models during all seasons. These results follow the established relationship between below-average precipitation and La Niña indicated in section 1. It is also important to note that some of the climate models analyzed indicate a relationship between MESA compound drought and heat and a negative phase of the IOD in autumn. Given the inconsistent relationships identified between the models, and that observations indicate no such relationship, the IOD was not further examined.

A comparison between different conditions in the climate models controlled by La Niña in the recent and prior periods revealed that atmospheric forcing by greenhouse gases and aerosols was principally responsible for heat during MESA compound drought and heat events and that La Niña was principally responsible for drought during these compound events. A comparison of recent and prior periods unconditioned on ENSO, which differ regarding their atmospheric forcing, indicates statistically significant increases in the frequency of MESA heat during all seasons that are unanimous across climate models, yet little change in the frequency of drought. A comparison of La Niña to El Niño and ENSO neutral (i.e., non–La Niña) both in the recent period from the climate models indicates statistically significant increases in the frequency of MESA drought during the autumn, winter, and spring wet seasons, but no consistent changes in the frequency of heat across the climate models. An important point to note is that the large temperature increases indicated by the climate models from the prior to recent period alone increase the frequency of compound drought and heat events without systematic shifts in precipitation to drier conditions. The effect of the large temperature shifts in the recent climate leads to compound drought and heat events in what would otherwise be a below-average precipitation and near-average temperature season in the prior period.

The climate model ensembles indicate that anthropogenic effects, through a comparison of recent and prior periods, did not lead to more MESA droughts since 1999. However, questions remain regarding anthropogenic effects on the zonal gradients in the equatorial Pacific Ocean, which are related to MESA precipitation (e.g., Hoell and Funk 2013), given the large differences between observed and model-simulated zonal gradients in the historical record (e.g., Coats and Karnauskas 2017; Olonscheck et al. 2020; Seager et al. 2022; Lee et al. 2022). Answers to these questions would affect our interpretation of anthropogenic effects on MESA precipitation, and therefore compound drought and heat events, and whether coupled climate models are appropriate for diagnosing these effects. The observed zonal Pacific SST gradients since 1900 have trended more La Niña–like (e.g., Cane et al. 1997; Karnauskas et al. 2009; Solomon and Newman 2012; L'Heureux et al. 2022), similar in some ways to the SST pattern related to MESA compound drought and heat (see also Barlow and Hoell 2015). By contrast, simulated zonal Pacific SST gradients trend more El Niño–like in most fully coupled climate models (e.g., Coats and Karnauskas 2017; Seager et al. 2022), which would lead to above-average MESA precipitation, given that El Niño increases the likelihood of above-average precipitation in western Asia. The differences between the observed and simulated trends attributed to variations internal to the climate system (Olonscheck et al. 2020; Deser et al. 2020) and/or model deficiencies (Seager et al. 2019, 2022) continue to be a matter of discussion (Power et al. 2021).

A goal of our study is to provide a situational awareness of conditions conducive to seasonal MESA compound drought and heat so that we may anticipate future occurrences. While knowledge of the drivers of such occurrences is part of providing a situational awareness, skillful forecasts of aspects of the causal chain are key, particularly as they relate to Pacific Ocean SSTs, given their variability on seasonal to decadal time scales (e.g., Di Lorenzo et al. 2023). A variety of techniques have been adopted to forecast Pacific SST many years in the future, and all have indicated some ability to skillfully predict conditions up to two years of lead time. These techniques include initialized dynamical model forecasts (e.g., Meehl et al. 2021; Choi and Son 2022; Hou et al. 2022) and climate model analogs in which forecasts are based on the evolution of SSTs in uninitialized climate model simulations from a state that most closely matches observations (Ding et al. 2018, 2019; Wang et al. 2020; Lou et al. 2023). Sustained improvements to our physical understanding and long-lead forecast skill in this MESA region are important to providing an early warning of hydroclimatic extremes where social dynamics, including food security, conflict, and migration, are sensitive to weather and climate.

Acknowledgments. The authors gratefully acknowledge two anonymous reviewers for constructive assessments and the Famine Early Warning Systems Network, the Bureau of Humanitarian Assistance, the U.S. Agency for International Development, and the NOAA Physical Sciences Laboratory for support. AH, RR, and M. Breeden were supported under the terms of AID-OFDA-T-17-00002. A.M. and K.S. were supported under the terms of PAPA 720BHA22H00005. The opinions expressed herein do not necessarily reflect the views of the U.S. Agency for International Development of the United States government.

Data availability statement. Observed estimates and transient climate model simulations were obtained from the sources documented in Tables 1 and 2, respectively.

REFERENCES

Abid, M. A., F. Kucharski, M. Almazroui, and I.-S. Kang, 2016: Interannual rainfall variability and ECMWF-Sys4-based predictability over the Arabian Peninsula winter monsoon region. *Quart. J. Roy. Meteor. Soc.*, **142**, 233–242, https://doi.org/10.1002/qj.2648.

——, M. Ashfaq, F. Kucharski, K. J. Evans, and M. Almazroui, 2020: Tropical Indian Ocean mediates ENSO influence over central southwest Asia during the wet season. *Geophys. Res. Lett.*, **47**, e2020GL089308, https://doi.org/10.1029/2020GL089308.

AghaKouchak, A., and Coauthors, 2020: Climate extremes and compound hazards in a warming world. *Annu. Rev. Earth*

Planet. Sci., **48**, 519–548, https://doi.org/10.1146/annurev-earth-071719-055228.

Agrawala, S., M. Barlow, H. Cullen, and B. Lyon, 2001: The drought and humanitarian crisis in central and southwest Asia: A climate perspective. IRI Special Rep. 01-11, 24 pp., https://doi.org/10.7916/D8NZ8FHQ.

Arias, P. A., and Coauthors, 2021: Technical summary. *Climate Change 2021: The Physical Science Basis*, V. Masson-Delmotte et al., Eds., Cambridge University Press, 33–144.

Athar, H., 2015: Teleconnections and variability in observed rainfall over Saudi Arabia during 1978–2010. *Atmos. Sci. Lett.*, **16**, 373–379, https://doi.org/10.1002/asl2.570.

Barlow, M., and A. Hoell, 2015: Drought in the Middle East and central–southwest Asia during winter 2013/14. *Bull. Amer. Meteor. Soc.*, **96**, S71–S76, https://doi.org/10.1175/BAMS-D-15-00127.1.

——, H. Cullen, and B. Lyon, 2002: Drought in central and southwest Asia: La Niña, the warm pool, and Indian Ocean precipitation. *J. Climate*, **15**, 697–700, https://doi.org/10.1175/1520-0442(2002)015<0697:DICASA>2.0.CO;2.

——, B. Zaitchik, S. Paz, E. Black, J. Evans, and A. Hoell, 2016: A review of drought in the Middle East and southwest Asia. *J. Climate*, **29**, 8547–8574, https://doi.org/10.1175/JCLI-D-13-00692.1.

——, A. Hoell, and L. Agel, 2021: An evaluation of CMIP6 historical simulations of the cold season teleconnection between tropical Indo-Pacific sea surface temperatures and precipitation in southwest Asia, the coastal Middle East, and northern Pakistan and India. *J. Climate*, **34**, 6905–6926, https://doi.org/10.1175/JCLI-D-19-1026.1.

Beck, H. E., N. E. Zimmermann, T. R. McVicar, N. Vergopolan, A. Berg, and E. F. Wood, 2018: Present and future Köppen-Geiger climate classification maps at 1-km resolution. *Sci. Data*, **5**, 180214, https://doi.org/10.1038/sdata.2018.214.

Breeden, M. L., J. R. Albers, and A. Hoell, 2022: Subseasonal precipitation forecasts of opportunity over southwest Asia. *Wea. Climate Dyn.*, **3**, 1183–1197, https://doi.org/10.5194/egusphere-2022-555.

Cane, M., and Coauthors, 1997: Twentieth-century sea surface temperature trends. *Science*, **275**, 957–960, https://doi.org/10.1126/science.275.5302.957.

Cannon, F., L. M. V. Carvalho, C. Jones, A. Hoell, J. Norris, G. N. Kiladis, and A. A. Tahir, 2017: The influence of tropical forcing on extreme winter precipitation in the western Himalaya. *Climate Dyn.*, **48**, 1213–1232, https://doi.org/10.1007/s00382-016-3137-0.

Capotondi, A., and Coauthors, 2015: Understanding ENSO diversity. *Bull. Amer. Meteor. Soc.*, **96**, 921–938, https://doi.org/10.1175/BAMS-D-13-00117.1.

Chakraborty, A., S. K. Behera, M. Mujumdar, R. Ohba, and T. Yamagata, 2006: Diagnosis of tropospheric moisture over Saudi Arabia and influences of IOD and ENSO. *Mon. Wea. Rev.*, **134**, 598–617, https://doi.org/10.1175/MWR3085.1.

Choi, J., and S.-W. Son, 2022: Seasonal-to-decadal prediction of El Niño–Southern Oscillation and Pacific decadal oscillation. *npj Climate Atmos. Sci.*, **5**, 29, https://doi.org/10.1038/s41612-022-00251-9.

Coats, S., and K. B. Karnauskas, 2017: Are simulated and observed twentieth century tropical Pacific sea surface temperature trends significant relative to internal variability? *Geophys. Res. Lett.*, **44**, 9928–9937, https://doi.org/10.1002/2017GL074622.

Danabasoglu, G., and Coauthors, 2020: The Community Earth System Model version 2 (CESM2). *J. Adv. Model. Earth Syst.*, **12**, e2019MS001916, https://doi.org/10.1029/2019MS001916.

Delworth, T. L., and Coauthors, 2020: SPEAR: The next generation GFDL modeling system for seasonal to multidecadal prediction and projection. *J. Adv. Model. Earth Syst.*, **12**, e2019MS001895, https://doi.org/10.1029/2019MS001895.

Deser, C., and Coauthors, 2020: Insights from Earth system model initial-condition large ensembles and future prospects. *Nat. Climate Change*, **10**, 277–286, https://doi.org/10.1038/s41558-020-0731-2.

Di Lorenzo, E., and Coauthors, 2023: Modes and mechanisms of Pacific decadal-scale variability. *Annu. Rev. Mar. Sci.*, **15**, 249–275, https://doi.org/10.1146/annurev-marine-040422-084555.

Ding, H., M. Newman, M. A. Alexander, and A. T. Wittenberg, 2018: Skillful climate forecasts of the tropical Indo-Pacific Ocean using model-analogs. *J. Climate*, **31**, 5437–5459, https://doi.org/10.1175/JCLI-D-17-0661.1.

——, ——, ——, and ——, 2019: Diagnosing secular variations in retrospective ENSO seasonal forecast skill using CMIP5 model-analogs. *Geophys. Res. Lett.*, **46**, 1721–1730, https://doi.org/10.1029/2018GL080598.

Efron, B., 1979: Bootstrap methods: Another look at the jackknife. *Ann. Stat.*, **7** (1), 1–26, https://doi.org/10.1214/aos/1176344552.

Eyring, V., S. Bony, G. A. Meehl, C. A. Senior, B. Stevens, R. J. Stouffer, and K. E. Taylor, 2016: Overview of the Coupled Model Intercomparison Project Phase 6 (CMIP6) experimental design and organization. *Geosci. Model Dev.*, **9**, 1937–1958, https://doi.org/10.5194/gmd-9-1937-2016.

Funk, C. C., and A. Hoell, 2015: The leading mode of observed and CMIP5 ENSO-residual sea surface temperatures and associated changes in Indo-Pacific climate. *J. Climate*, **28**, 4309–4329, https://doi.org/10.1175/JCLI-D-14-00334.1.

Gerlitz, L., E. Steirou, C. Schneider, V. Moron, S. Vorogushyn, and B. Merz, 2018: Variability of the cold season climate in central Asia. Part I: Weather types and their tropical and extratropical drivers. *J. Climate*, **31**, 7185–7207, https://doi.org/10.1175/JCLI-D-17-0715.1.

——, ——, ——, ——, ——, and ——, 2019: Variability of the cold season climate in central Asia. Part II: Hydroclimatic predictability. *J. Climate*, **32**, 6015–6033, https://doi.org/10.1175/JCLI-D-18-0892.1.

Giorgi, F., 2006: Climate change hot-spots. *Geophys. Res. Lett.*, **33**, L08707, https://doi.org/10.1029/2006GL025734.

Gleick, P. H., 2014: Water, drought, climate change, and conflict in Syria. *Wea. Climate Soc.*, **6**, 331–340, https://doi.org/10.1175/WCAS-D-13-00059.1.

Harris, I., T. J. Osborn, P. Jones, and D. Lister, 2020: Version 4 of the CRU TS monthly high-resolution gridded multivariate climate dataset. *Sci. Data*, **7**, 109, https://doi.org/10.1038/s41597-020-0453-3.

Hersbach, H., and Coauthors, 2020: The ERA5 global reanalysis. *Quart. J. Roy. Meteor. Soc.*, **146**, 1999–2049, https://doi.org/10.1002/qj.3803.

Hoell, A., and C. Funk, 2013: The ENSO-related west Pacific sea surface temperature gradient. *J. Climate*, **26**, 9545–9562, https://doi.org/10.1175/JCLI-D-12-00344.1.

——, M. Barlow, and R. Saini, 2012: The leading pattern of intraseasonal and interannual Indian Ocean precipitation variability and its relationship with Asian circulation during the boreal cold season. *J. Climate*, **25**, 7509–7526, https://doi.org/10.1175/JCLI-D-11-00572.1.

——, ——, and ——, 2013: Intraseasonal and seasonal-to-interannual Indian Ocean convection and hemispheric teleconnections. *J. Climate*, **26**, 8850–8867, https://doi.org/10.1175/JCLI-D-12-00306.1.

——, C. Funk, and M. Barlow, 2014a: The regional forcing of Northern Hemisphere drought during recent warm tropical west Pacific Ocean La Niña events. *Climate Dyn.*, **42**, 3289–3311, https://doi.org/10.1007/s00382-013-1799-4.

——, ——, and ——, 2014b: La Niña diversity and northwest Indian Ocean rim teleconnections. *Climate Dyn.*, **43**, 2707–2724, https://doi.org/10.1007/s00382-014-2083-y.

——, ——, and ——, 2015a: The forcing of southwestern Asia teleconnections by low-frequency sea surface temperature variability during boreal winter. *J. Climate*, **28**, 1511–1526, https://doi.org/10.1175/JCLI-D-14-00344.1.

——, S. Shukla, M. Barlow, F. Cannon, C. Kelley, and C. Funk, 2015b: The forcing of monthly precipitation variability over southwest Asia during the boreal cold season. *J. Climate*, **28**, 7038–7056, https://doi.org/10.1175/JCLI-D-14-00757.1.

——, M. Barlow, F. Cannon, and T. Xu, 2017a: Oceanic origins of historical southwest Asia precipitation during the boreal cold season. *J. Climate*, **30**, 2885–2903, https://doi.org/10.1175/JCLI-D-16-0519.1.

——, C. Funk, M. Barlow, and F. Cannon, 2017b: A physical model for extreme drought over southwest Asia. *Climate Extremes: Patterns and Mechanisms*, *Geophys. Monogr.*, Vol. 226, Amer. Geophys. Union, 283–298, https://doi.org/10.1002/9781119068020.ch17.

——, M. Barlow, T. Xu, and T. Zhang, 2018: Cold season southwest Asia precipitation sensitivity to El Niño–Southern Oscillation events. *J. Climate*, **31**, 4463–4482, https://doi.org/10.1175/JCLI-D-17-0456.1.

——, J. Eischeid, M. Barlow, and A. McNally, 2020: Characteristics, precursors, and potential predictability of Amu Darya drought in an Earth system model large ensemble. *Climate Dyn.*, **55**, 2185–2206, https://doi.org/10.1007/s00382-020-05381-5.

Hoskins, B. J., and K. I. Hodges, 2019: The annual cycle of Northern Hemisphere storm tracks. Part I: Seasons. *J. Climate*, **32**, 1743–1760, https://doi.org/10.1175/JCLI-D-17-0870.1.

Hou, Z., J. Li, R. Ding, and J. Feng, 2022: Investigating decadal variations of the seasonal predictability limit of sea surface temperature in the tropical Pacific. *Climate Dyn.*, **59**, 1079–1096, https://doi.org/10.1007/s00382-022-06179-3.

Huang, B., and Coauthors, 2017: Extended Reconstructed Sea Surface Temperature, version 5 (ERSSTv5): Upgrades, validations, and intercomparisons. *J. Climate*, **30**, 8179–8205, https://doi.org/10.1175/JCLI-D-16-0836.1.

Kang, I.-S., I. U. Rashid, F. Kucharski, M. Almazroui, and A. K. Alkhalaf, 2015: Multidecadal changes in the relationship between ENSO and wet-season precipitation in the Arabian Peninsula. *J. Climate*, **28**, 4743–4752, https://doi.org/10.1175/JCLI-D-14-00388.1.

Kaniewski, D., E. Van Campo, and H. Weiss, 2012: Drought is a recurring challenge in the Middle East. *Proc. Natl. Acad. Sci. USA*, **109**, 3862–3867, https://doi.org/10.1073/pnas.1116304109.

Karnauskas, K. B., R. Seager, A. Kaplan, Y. Kushnir, and M. A. Cane, 2009: Observed strengthening of the zonal sea surface temperature gradient across the equatorial Pacific Ocean. *J. Climate*, **22**, 4316–4321, https://doi.org/10.1175/2009JCLI2936.1.

Kay, J. E., and Coauthors, 2015: The Community Earth System Model (CESM) large ensemble project: A community resource for studying climate change in the presence of internal climate variability. *Bull. Amer. Meteor. Soc.*, **96**, 1333–1349, https://doi.org/10.1175/BAMS-D-13-00255.1.

Kelley, C. P., S. Mohtadi, M. A. Cane, R. Seager, and Y. Kushnir, 2015: Climate change in the Fertile Crescent and implications of the recent Syrian drought. *Proc. Natl. Acad. Sci. USA*, **112**, 3241–3246, https://doi.org/10.1073/pnas.1421533112.

Lautze, S., E. Stites, N. Nojumi, and F. Najimi, 2002: Qaht-E-Pool "A cash famine": Food insecurity in Afghanistan 1999–2002. Feinstein International Famine Center Rep., 61 pp., https://reliefweb.int/attachments/788afb69-e636-3551-b31d-63663a459840/9267090F31843C2B85256BD4005731B6-tufts-afg-07june.pdf.

Lee, S., M. L'Heureux, A. T. Wittenberg, R. Seager, P. A. O'Gorman, and N. C. Johnson, 2022: On the future zonal contrasts of equatorial Pacific climate: Perspectives from observations, simulations, and theories. *npj Climate Atmos. Sci.*, **5**, 82, https://doi.org/10.1038/s41612-022-00301-2.

L'Heureux, M. L., M. K. Tippett, and W. Wang, 2022: Prediction challenges from errors in tropical Pacific sea surface temperature trends. *Front. Climate*, **4**, 837483, https://doi.org/10.3389/fclim.2022.837483.

Lou, J., M. Newman, and A. Hoell, 2023: Multi-decadal variation of ENSO forecast skill since the late 1800s. *npj Climate Atmos. Sci.*, **6**, 89, https://doi.org/10.1038/s41612-023-00417-z.

Mantua, N. J., S. R. Hare, Y. Zhang, J. M. Wallace, and R. C. Francis, 1997: A Pacific interdecadal climate oscillation with impacts on salmon production. *Bull. Amer. Meteor. Soc.*, **78**, 1069–1080, https://doi.org/10.1175/1520-0477(1997)078<1069:APICOW>2.0.CO;2.

Mariotti, A., 2007: How ENSO impacts precipitation in southwest central Asia. *Geophys. Res. Lett.*, **34**, L16706, https://doi.org/10.1029/2007GL030078.

Mauritsen, T., and Coauthors, 2019: Developments in the MPI-M Earth System Model version 1.2 (MPI-ESM1.2) and its response to increasing CO_2. *J. Adv. Model. Earth Syst.*, **11**, 998–1038, https://doi.org/10.1029/2018MS001400.

McNally, A., and Coauthors, 2022: A central Asia hydrologic monitoring dataset for food and water security applications in Afghanistan. *Earth Syst. Sci. Data*, **14**, 3115–3135, https://doi.org/10.5194/essd-14-3115-2022.

Meehl, G. A., and Coauthors, 2021: Initialized Earth system prediction from subseasonal to decadal timescales. *Nat. Rev. Earth Environ.*, **2**, 340–357, https://doi.org/10.1038/s43017-021-00155-x.

Mukherjee, S., and A. K. Mishra, 2021: Increase in compound drought and heatwaves in a warming world. *Geophys. Res. Lett.*, **48**, e2020GL090617, https://doi.org/10.1029/2020GL090617.

Nazemosadat, M. J., and A. R. Ghasemi, 2004: Quantifying the ENSO-related shifts in the intensity and probability of drought and wet periods in Iran. *J. Climate*, **17**, 4005–4018, https://doi.org/10.1175/1520-0442(2004)017<4005:QTESIT>2.0.CO;2.

Newman, M., and Coauthors, 2016: The Pacific decadal oscillation, revisited. *J. Climate*, **29**, 4399–4427, https://doi.org/10.1175/JCLI-D-15-0508.1.

Olonscheck, D., M. Rugenstein, and J. Marotzke, 2020: Broad consistency between observed and simulated trends in sea surface temperature patterns. *Geophys. Res. Lett.*, **47**, e2019GL086773, https://doi.org/10.1029/2019GL086773.

Power, S., and Coauthors, 2021: Decadal climate variability in the tropical Pacific: Characteristics, causes, predictability, and prospects. *Science*, **374**, eaay9165, https://doi.org/10.1126/science.aay9165.

Rana, S., J. McGregor, and J. Renwick, 2017: Wintertime precipitation climatology and ENSO sensitivity over central southwest Asia. *Int. J. Climatol.*, **37**, 1494–1509, https://doi.org/10.1002/joc.4793.

Rodgers, K. B., and Coauthors, 2021: Ubiquity of human-induced changes in climate variability. *Earth Syst. Dyn.*, **12**, 1393–1411, https://doi.org/10.5194/esd-12-1393-2021.

Rohde, R. A., and Z. Hausfather, 2020: The Berkeley Earth land/ocean temperature record. *Earth Syst. Sci. Data*, **12**, 3469–3479, https://doi.org/10.5194/essd-12-3469-2020.

Saji, N. H., B. N. Goswami, P. N. Vinayachandran, and T. Yamagata, 1999: A dipole mode in the tropical Indian Ocean. *Nature*, **401**, 360–363, https://doi.org/10.1038/43854.

Schneider, U., P. Finger, A. Meyer-Christoffer, E. Rustemeier, M. Ziese, and A. Becker, 2017: Evaluating the hydrological cycle over land using the newly-corrected precipitation climatology from the Global Precipitation Climatology Centre (GPCC). *Atmosphere*, **8**, 52, https://doi.org/10.3390/atmos8030052.

Seager, R., M. Cane, N. Henderson, D.-E. Lee, R. Abernathey, and H. Zhang, 2019: Strengthening tropical Pacific zonal sea surface temperature gradient consistent with rising greenhouse gases. *Nat. Climate Change*, **9**, 517–522, https://doi.org/10.1038/s41558-019-0505-x.

——, N. Henderson, and M. Cane, 2022: Persistent discrepancies between observed and modeled trends in the tropical Pacific Ocean. *J. Climate*, **35**, 4571–4584, https://doi.org/10.1175/JCLI-D-21-0648.1.

Selby, J., and C. Hoffmann, 2012: Water scarcity, conflict, and migration: A comparative analysis and reappraisal. *Environ. Plann. C*, **30**, 997–1014, https://doi.org/10.1068/c11335j.

Solomon, A., and M. Newman, 2012: Reconciling disparate twentieth-century Indo-Pacific ocean temperature trends in the instrumental record. *Nat. Climate Change*, **2**, 691–699, https://doi.org/10.1038/nclimate1591.

Taylor, K. E., R. J. Stouffer, and G. A. Meehl, 2012: An overview of CMIP5 and the experiment design. *Bull. Amer. Meteor. Soc.*, **93**, 485–498, https://doi.org/10.1175/BAMS-D-11-00094.1.

Tebaldi, C., J. M. Arblaster, and R. Knutti, 2011: Mapping model agreement on future climate projections. *Geophys. Res. Lett.*, **38**, L23701, https://doi.org/10.1029/2011GL049863.

Timmermann, A., and Coauthors, 2018: El Niño–Southern Oscillation complexity. *Nature*, **559**, 535–545, https://doi.org/10.1038/s41586-018-0252-6.

Tripathy, K. P., S. Mukherjee, A. K. Mishra, M. E. Mann, and A. P. Williams, 2023: Climate change will accelerate the high-end risk of compound drought and heatwave events. *Proc. Natl. Acad. Sci. USA*, **120**, e2219825120, https://doi.org/10.1073/pnas.2219825120.

Wang, Y., Z. Zhang, and P. Huang, 2020: An improved model-based analogue forecasting for the prediction of the tropical Indo-Pacific sea surface temperature in a coupled climate model. *Int. J. Climatol.*, **40**, 6346–6360, https://doi.org/10.1002/joc.6584.

Wieners, K.-H., and Coauthors, 2019a: MPI-M MPI-ESM1.2-LR model output prepared for CMIP6 ScenarioMIP ssp585. Earth System Grid Federation, accessed 1 March 2021, https://doi.org/10.22033/ESGF/CMIP6.6705.

——, and Coauthors, 2019b: MPI-M MPI-ESM1.2-LR model output prepared for CMIP6 CMIP historical. Earth System Grid Federation, accessed 1 March 2021, https://doi.org/10.22033/ESGF/CMIP6.6595.

Xu, X., L. Wang, and W. Yu, 2021: The unique mean seasonal cycle in the Indian Ocean anchors its various air-sea coupled modes across the basin. *Sci. Rep.*, **11**, 5632, https://doi.org/10.1038/s41598-021-84936-w.

Zhang, J., and Coauthors, 2021: The role of anthropogenic aerosols in the anomalous cooling from 1960 to 1990 in the CMIP6 Earth system models. *Atmos. Chem. Phys.*, **21**, 18 609–18 627, https://doi.org/10.5194/acp-21-18609-2021.

Zhang, W., M. Luo, S. Gao, W. Chen, V. Hari, and A. Khouakhi, 2021: Compound hydrometeorological extremes: Drivers mechanisms and methods. *Front. Earth Sci.*, **9**, 673495, https://doi.org/10.3389/feart.2021.673495.

Zscheischler, J., and Coauthors, 2018: Future climate risk from compound events. *Nat. Climate Change*, **8**, 469–477, https://doi.org/10.1038/s41558-018-0156-3.

——, and Coauthors, 2020: A typology of compound weather and climate events. *Nat. Rev. Earth Environ.*, **1**, 333–347, https://doi.org/10.1038/s43017-020-0060-z.